

Aragonite crystal orientation in mollusk shell nacre may depend on temperature. The angle spread of crystalline aragonite tablets records the water temperature at which nacre was deposited by *Pinctada margaritifera*

Ian C. Olson^a and Pupa U. P. A. Gilbert^{*b}

Received 6th March 2012, Accepted 6th June 2012

DOI: 10.1039/c2fd20047c

Nacre, or mother-of-pearl, is a lamellar composite of aragonite (CaCO_3) tablets with a broad distribution of angular orientations. The angle spread is the full-width of this distribution. Here we analysed the angle spread as a function of position in the nacre layer of one *Pinctada margaritifera* shell, compared the results with temperature data, and found these two parameters to be highly correlated. This result suggests that one could calculate the temperature at which nacre formed by measuring only its angle spread. Validation of the correlation in modern and ancient nacre from other species is necessary, but if confirmed, nacre could provide a physical proxy for temperature in modern and ancient climates.

1 Introduction

Nacre is a composite of aragonite (CaCO_3) tablets and organic sheets, alternating to form a lamellar structure at the inner side of several mollusc shells,¹ including those made by gastropods (for instance, trochus, turbo, abalone, but not whelk, nor conch, nor cowrie, nor conus), one cephalopod (*Nautilus*), and a few bivalves (all *Mytilus* mussels, *Pinctada* pearl oysters, pen shells, but not clams or scallops). Previously nacre was believed to have perfectly co-oriented crystalline tablets, with their crystallographic *c*-axes parallel to the normal to the nacre layers. In recent years our group² and others³ have observed that nacre tablets have a wide distribution of *c*-axis orientations, centred about the normal. The width of this distribution, termed angle spread, varies across species.^{2f} In Fig. 1 we present three polarization-dependent imaging contrast maps, or PIC-maps, from different shells, and their *c'*-axis distributions.

If the tablet *c*-axes in nacre were co-oriented as previously believed, in PIC-maps such as those in Fig. 1 they would exhibit no contrast and all tablets would appear homogeneously gray.

The difference in angle spread across species stimulated our interest and a quest for the environmental parameters that might correlate with angle spread in nacre tablets. We found a strong direct correlation ($R = 0.77$) between the angle spread and the maximum temperature at which a mollusc species lives. Specifically, we found that the greater the maximum temperature the greater the angle spread measured in nacre.^{2f} However, the meaning and scope of the observed correlation

^aDepartment of Physics, University of Wisconsin, Madison, WI, 53706, USA. E-mail: iolson@wisc.edu; Fax: +1 608 265 2334; Tel: +1 608 265 3767

^bDepartments of Physics and Chemistry, University of Wisconsin, Madison, WI, 53706, USA. E-mail: pupa@physics.wisc.edu; Fax: +1 608 265 2334; Tel: +1 608 262 5829

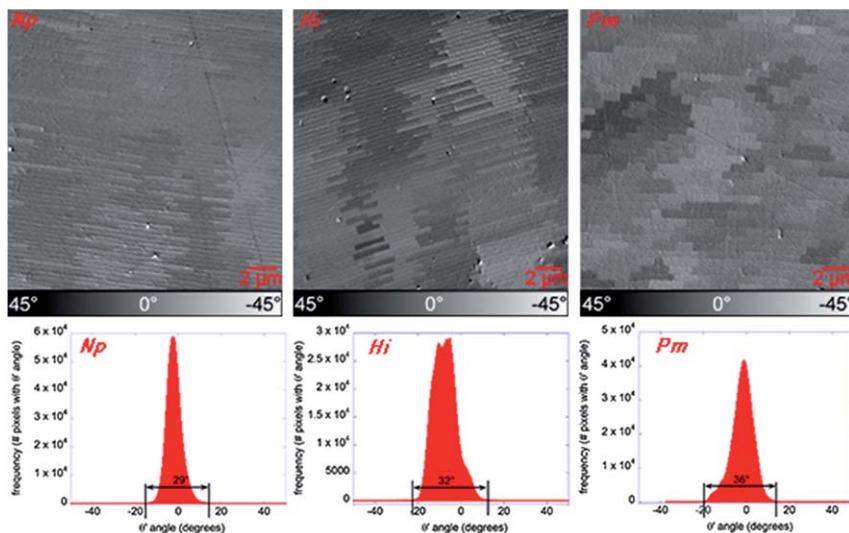


Fig. 1 Polarization-dependent imaging contrast maps (PIC-maps) from three mollusc shells: the cephalopod *Nautilus pompilius* (*Np*), the gastropod *Haliotis iris* (*Hi*), and the bivalve *Pinctada margaritifera* (*Pm*). In a PIC-map different gray levels represent different crystal *c*-axis orientations.⁴ PIC-mapping has a spatial resolution of 20 nm, and $\sim 2^\circ$ resolution for discriminating different orientations of the *c'*-axis, that is, the angle θ' formed by the projection of the aragonite crystal *c*-axis onto the plane in which the polarization vector of the illuminating X-rays rotates.^{2f,5} Within this resolution each nacre tablet behaves as a single crystal. Columns of tablets stacked on top of one another share the same orientation in gastropod and cephalopod columnar nacre, *e.g.* in *Np* and *Hi*. Conversely, stacks of co-oriented tablets appear to be staggered laterally in sheet nacre from bivalves, *e.g.* in *Pm*. The histogram under each PIC-map shows the frequency at which each θ' angle or gray level is measured, across all the $10^3 \times 10^3$ pixels in the PIC-map. The footprint of the distribution provides a measurement of how much the *c'*-axes can vary in their orientations, which we define here as the angle spread. The angle spread varies across species, as shown here in the histograms in *Np*, *Hi*, and *Pm* and in previous work across 8 species.^{2f}

remained unclear. It was possible that the angle spread became larger as a result of adaptation to varying temperature over long time periods, as climates changed, as molluscs themselves migrated to different climates, or as continental drift or other geologic phenomena brought the molluscs into new environmental temperatures. It was also possible that the angle spread reacted rapidly to changing water temperature, during the life of a single animal. To test these hypotheses we did the experiments described here, in which one mollusc shell was analysed with secondary ion mass spectrometry (SIMS) and then the same shell locations measured with SIMS were analysed with PIC-mapping to measure the angle spread.

2 Results

In Fig. 2 we present the *Pinctada margaritifera* shell analysed with both SIMS and PIC-mapping. In Fig. 3 we present three specific areas α , β , and γ , located respectively at the beginning, the middle, and the end of the region analysed by PIC-mapping and SIMS, and also shown in Fig. 2. The PIC mapping results for angle spread as a function of position in the shell, acquired from these and many more locations are presented in Fig. 4, where they are also compared with the temperature data recorded by a National Oceanic and Atmospheric Administration (NOAA) buoy,⁶ 25 m under the water surface, from a location less than 1000 km from French Polynesia, where the shell grew.



Fig. 2 Cross-polarizer, reflected light micrograph of a *Pinctada margaritifera* shell, embedded in epoxy and polished to expose a cross-section with the calcite prismatic layer at the bottom third, and the nacre layer in the top two thirds of the shell. Beginning at the inner surface of the shell (top), the nacre layer was analysed for oxygen isotope ratio with SIMS, with one 10- μm SIMS pit every 10 μm , in a zig-zag pattern to avoid overlapping, extending ~ 2.4 mm into the shell.^{2f} The ~ 240 SIMS pits are visible in this image as a faint vertical gray line. A shorter distance, extending ~ 1.3 mm was also analysed with PIC-mapping. The arrows point towards three regions at the beginning (α) the middle (β) and the end (γ) of the region analysed by both SIMS and PIC-mapping. The nacre layer has a gap between α and β , where the shell was broken during sample preparations.

Based on the striking match of angle spread and temperature data, we may have established a correspondence between position in the shell and its time of formation. This is quantitatively described by the equation in Fig. 4 caption. We must now verify that the rest of the data deduced by the visual matching of the two curves are reasonable. We do so by first comparing in Table 1 the complete set of data measured in positions α , β , and γ , using these data to measure the nacre growth rate, then using the match in Fig. 4 to plot $\delta^{18}\text{O}$ and angle spread, or $\delta^{18}\text{O}$ and temperature data as a function of time (Fig. 5, 6), and finally plotting temperature as a function of angle-spread (Fig. 7).

Using the data in Table 1, we can see that between point α and point γ the distance is $2358 - 1043 = 1315$ μm , and these points formed $3457 - 1514 = 1943$ days apart from one another. Therefore the shell grew precisely $1315/1943 = 0.68$ $\mu\text{m day}^{-1}$. This number is in remarkable agreement with the tablet thicknesses described by Olson *et al.*: 0.66 μm , 0.67 μm , and 0.68 μm average tablet thicknesses in different regions of *Pm*.^{2f} This result strongly suggests that one tablet-layer per day is deposited by *Pm*. Furthermore, it confirms that the match of Fig. 4 is not unreasonable, as nacre layers may very well be correlated with the mollusc's circadian rhythm.

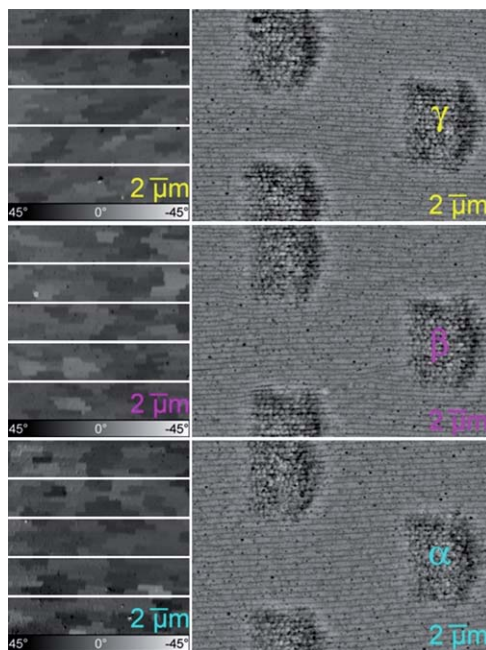


Fig. 3 On the right hand side we show back-scattered electron SEM micrographs of the pits left in nacre by SIMS analysis, each approximately 10 μm in size, from which aragonite desorbed and the corresponding stable oxygen isotope concentrations were measured. The pits labelled α , β , and γ are the same shown at lower magnification in Fig. 2. On the left hand side we present PIC-maps, acquired in 20 $\mu\text{m} \times 20 \mu\text{m}$ regions immediately adjacent to the α , β , and γ pits, each subdivided into 5 slices of 4 $\mu\text{m} \times 20 \mu\text{m}$ to provide more data points with angle spread analysis.

Assuming that the time-position relationship in Fig. 4 is correct, we can now plot the SIMS results as a function of date, and compare them with the angle spread results also plotted as a function of date, as presented in Fig. 5.

In Fig. 6 we compare $\delta^{18}\text{O}$ data with temperature. The $\delta^{18}\text{O}$ is expected to be anti-correlated with temperature in abiotic⁷ and biomineral systems.^{7c,8}

In order to compare $\delta^{18}\text{O}$ and temperature data in Fig. 6 we assumed that the ratio of oxygen isotope concentrations ($^{18}\text{O}/^{16}\text{O}$), expressed as $\delta^{18}\text{O}$ of the seawater in which the shell was formed did not change during the shell formation time. This assumption, which is in fact not true experimentally,^{7b-c} is used here as a simplification, and because the necessary reference $\delta^{18}\text{O}$ data from the seawater were not available. If they were available, the non-constant $\delta^{18}\text{O}$ would remove fluctuations observed in Fig. 6 that are not real temperature changes. With the imperfect assumption that $\delta^{18}\text{O}$ of seawater did not change, however, the minima in $\delta^{18}\text{O}$ correspond to the maxima in temperature,^{7a,7c,9} and *vice versa*. The data of Fig. 6 show such correspondence in 7 time points and their surroundings. This is a worse match than that in Fig. 4. The discrepancy, however, may be due to variations in seawater $\delta^{18}\text{O}$.

Since the angle spread and temperature curves as a function of time match so nicely (Fig. 4), we attempt here a data regression, that is, a plot of these two parameters *versus* one another. In Fig. 7 we present such data: the temperature data as a function of angle spread.

The strong correlation of water temperature and angle spread is evidenced by the linear fit in Fig. 7 and the high correlation coefficient ($R = 0.704$). In addition, the fit in Fig. 7 provides an equation according to which one can calculate the temperature

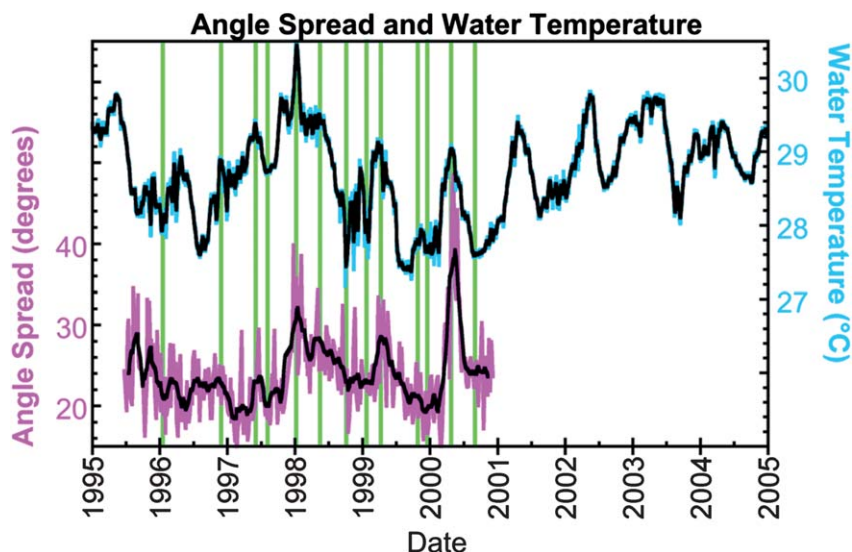


Fig. 4 Angle spread results as a function of position in the shell (magenta curve, bottom), compared with temperature data as a function of time (cyan curve, top), recorded once per day by a NOAA buoy. Each date year is placed in the position of January 1st of that year. Notice that the growth rate of the shell was unknown, and so was the mollusc's death time. The only certain data point was that the shell was acquired by one of us in 2004, and must therefore have formed before then. We smoothed both the angle-spread curve and the temperature curve over 9 points (black curves) to facilitate identification of slopes, peaks, dips, and similitude of the two curves. We then stretched the horizontal scale of the angle-spread curve, and shifted it, until the two curves matched, as judged visually. The stretching done was then quantified according to the equation: $\text{Time} = -44.65 \text{ days} + 1.48 \frac{\text{days}}{\mu\text{m}} \times \text{position [in } \mu\text{m}]$, where Time is the time of nacre formation, measured in days before January 1st, 2005. Notice that the temperature data are not perfectly reproducible in subsequent years, nor are the angle spread data, and both curves have a great deal of noise. The two curves however have a remarkable similitude. At the time points in which we observe alignment of maxima or minima in the two curves, we placed a green vertical line behind the curves. There are 13 time points in which peak-peak or dip-dip similitude is observed, and around these time points the slopes of the two curves are in striking agreement.

Table 1 Complete set of data measured directly in PIC-mapping or SIMS (angle spread, or $\delta^{18}\text{O}$, respectively) or deduced using the match in Fig. 4 (date, temperature)

Parameter measured	Point α	Point β	Point γ
Days before Jan 1st, 2005	3457	2489	1514
Date (mm/dd/yyyy)	07/15/1995	03/09/1998	11/08/2000
Position	2358 μm	1703 μm	1043 μm
Angle spread (smoothed over 9pt)	24.0°	26.6°	23.6°
SIMS pit number	386	296	212
$\delta^{18}\text{O}$ (‰, smoothed over 5pt)	-3.2	-2.7	-2.7
T (at 25m depth)	28.86 °C	29.32 °C	27.78 °C

at which the nacre formed (T) from the measured angle spread (AS). The equation is: $T = 26.738 + 0.050 AS$. Using this simple linear equation nacre in *Pinctada margaritifera* can be used as a thermometer. In Fig. 7 we only plotted 15 months of data. If we plot the entire range of data available (5.3 years) the linear fit is similar (the

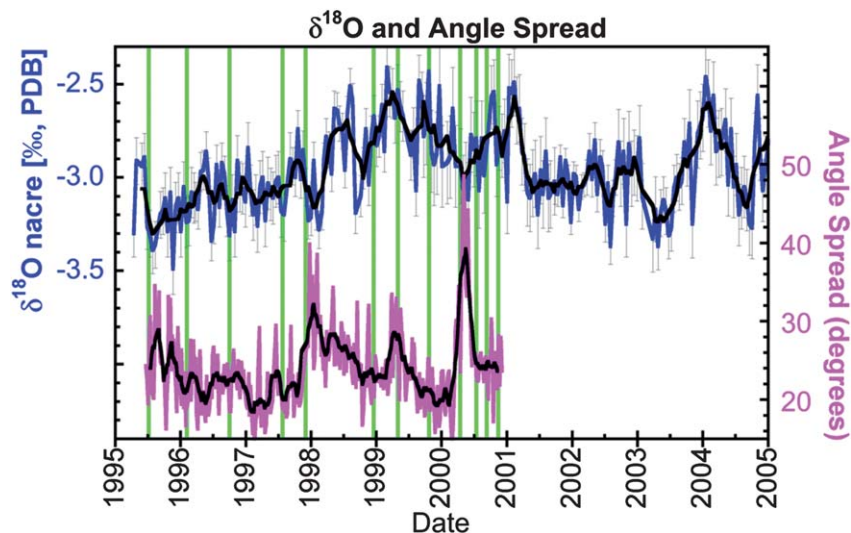


Fig. 5 Comparison of the stable oxygen isotope concentration ratio [^{18}O]/[^{16}O], expressed as $\delta^{18}\text{O}$ of nacre. To facilitate comparison, the black lines indicate smoothed curves, over 9 and 5 points for angle spread and $\delta^{18}\text{O}$, respectively. The $\delta^{18}\text{O}$ increases when the temperature decreases, hence peaks in $\delta^{18}\text{O}$ should correspond to dips in angle spread and *vice versa*. Indeed we observe good anti-correlation at the 12 time points indicated by green vertical lines.

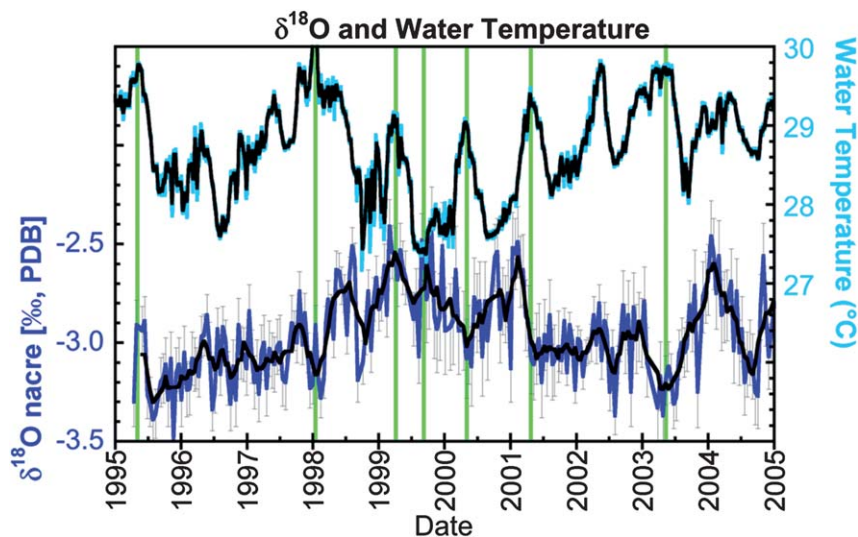


Fig. 6 Comparison of $\delta^{18}\text{O}$ of nacre and water temperature data, both as a function of date. Again we have smoothed both curves (black lines) over 5 and 9 points respectively. The $\delta^{18}\text{O}$ is expected to increase as the temperature decreases, hence the maxima and minima in these two curves should align. The two curves are far from being the mirror image of one another. However there is acceptable anti-correlation at the 7 time points indicated by green vertical lines.

intercept is $27.631\text{ }^{\circ}\text{C}$ and the slope $0.035\text{ }^{\circ}\text{C}/\text{‰}$, but the correlation coefficient is far worse ($R = 0.29$). We believe that this problem results from acquiring angle spread data from regions $4\text{ }\mu\text{m} \times 20\text{ }\mu\text{m}$ (Fig. 2). Such small images contain too few tablets to provide a statistically representative histogram of angles and angle spread. The angle spread data, therefore, are under-sampled. Much larger fields of view must

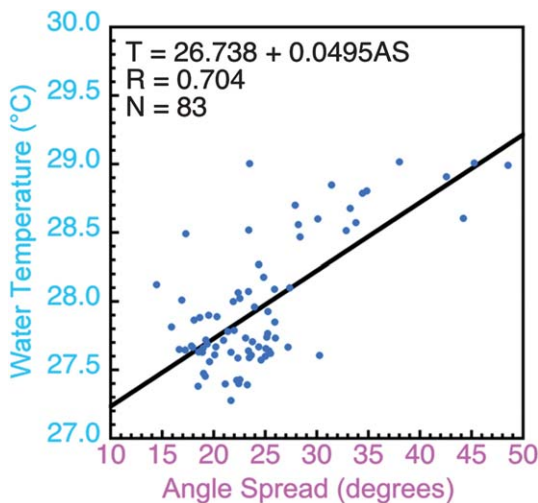


Fig. 7 The water temperature data plotted *versus* the angle spread data for dates between 8/7/1999 and 11/8/2000. Note that the 83 data points are fitted by a line with slope $0.050\text{ }^{\circ}\text{C}/^{\circ}$, and intercept $26.738\text{ }^{\circ}\text{C}$. The fit gives a high correlation coefficient $R = 0.704$.

be used in future PIC-maps to resolve this problem. Acquiring such data is entirely feasible, but has not been done. Only the detailed analysis done here revealed the existence of a sampling problem, and paved the way for possible future development of nacre-thermometry. Whether the above equation applies to other modern shells, or to ancient nacre from extinct mollusc species remains to be determined.

3 Discussion

We have explored for the first time the possibility that a structural parameter in nacre, that is, the angle spread of its aragonite tablets, is correlated with the water temperature at the time in which the mollusc deposited the shell mineral. We have found a remarkably good agreement between the angle spread and the temperature curves, both plotted as a function of time as shown in Fig. 4. By comparison, the values of $\delta^{18}\text{O}$ here gave worse agreement with both angle spread and temperature data as a function of time (Fig. 5 and 6). If the match of angle spread and temperature data attempted in Fig. 4 is correct, then the angle spread is highly correlated with water temperature. This correlation strongly suggests that nacre angle spread could be used to determine the water temperature at the time a mollusc deposited its shell. The data regression of Fig. 7 further supports this suggestion. The temperature-angle spread correlation is certainly true in one *Pm* shell, as shown here, but must be confirmed on many more shells, from different species and locations, with known times of death and local temperatures, or grown in aquaria with controlled conditions. Larger fields of view (*e.g.* $80\text{ }\mu\text{m} \times 40\text{ }\mu\text{m}$) will improve angle-spread sampling at each location in the shell, corresponding to each formation time and temperature. In addition, mollusc shells formed in locations or aquaria in which the temperatures vary by a greater interval than that tested here (3°) will provide much stronger evidence and more stable linear fits, with slope and intercept not fluctuating depending on sampling. It is possible that, after all this future work is done, the linear equation correlating angle spread and temperature will differ from the one reported here in Fig. 7.

The question raised above on the time-scale of the angle-spread and temperature correlation is addressed by the data presented here, and these data are sufficient to

rule out the possibility that adaptations in angle spread took place over a very long time period of mollusc evolution in changing climates. The increase/decrease in angle spread takes place each day during the life of the mollusc, in response to increasing/decreasing water temperature.

Why does the angle spread increase when the temperature increases? Abiotically carbonate crystals grow faster at higher temperature.¹⁰ It is possible that this is the case also in biogenic aragonite in nacre, but this is not known. If crystals grow faster at higher temperatures, it is possible that the proteins controlling crystal growth in specific directions,¹¹ and therefore crystal orientations,²⁷ cannot be produced fast enough by the organism, and therefore greater disorder and angle spread ensue. The opposite is also possible: an increased temperature provokes increased metabolic rate, which makes the organism produce more and better organic molecules. This would result in greater angle spread if this was advantageous for the organism. It is unknown at present whether co-orientation or mis-orientation of tablets provides an evolutionary advantage.

The angle spread was measured in this work using PIC-mapping. However, this may not be the best method to measure angle spreads, as using a microscope and then clumping together all tablet orientation angles and measuring their maximum angle spread is unnecessarily complex. More directly averaged angle-spread results could be obtained in X-ray diffraction experiments by measuring the footprint of a rocking curve,^{28,12} or the footprint of a pole figure,¹³ or using the March-Dollase approach.¹⁴ In scanning electron microscopy angle spreads can be measured by electron back-scattered diffraction,¹⁵ or by direct imaging of partly etched tablets.¹⁶ This has not been tested, but in principle one or more of these methods could provide nacre angle-spread proxies for temperature.

Future work will determine if nacre can be used as a proxy for temperature, as suggested by the data here. Most other temperature proxies are chemical in nature, that is, they measure ratios of concentrations of different minerals (*e.g.* aragonite/calcite ratio¹⁷) or different elements (*e.g.* [Mg]/[Ca]¹⁸), or ratios of concentrations of different isotopes of the same element (*e.g.* $\delta^{18}\text{O}$ ¹⁹), or clumped isotopes of multiple elements.²⁰ If confirmed and validated on other shells and different growth temperatures, this could be one of only a few physical proxies, along with porosity in foraminifera, which depends on temperature.²¹

A physical proxy may have advantages and disadvantages. It is more sensitive than a chemical proxy to diagenetic structural changes. Diagenesis in nacre manifests as dissolution²² or dissolution and recrystallization as calcite²³ or hydroxyapatite.²⁴ However, when either of these phenomena occur, nacre's layering and physical structure is poorly preserved at the microscopic scale, hence these problems will be evident from images and spectra in the photoelectron emission spectromicroscopy (PEEM) experiment used for PIC-mapping. It is thereby easy to select only layered, aragonite regions of well-preserved nacre²⁵ for the measurement of angle spread. An advantage of a physical proxy is that, if the structure is preserved, chemical changes such as elemental losses or enrichments do not affect the angle-spread measurement, thus this method is expected to be less artifact-prone compared to chemical proxies.

We have shown here that angle-spread is a proxy for temperature in *modern* nacre from one shell, and, if validated in other modern and ancient shells, could become a valuable temperature proxy. This possibility is most intriguing when one considers that nacre is abundant in the fossil record (*e.g.* in ammonites) spanning 450 million years.²⁶ If the same *fossil* nacre can be analysed with the present technique and other temperature proxies, nacre could be validated not only as a thermometer, but also as a paleothermometer. Unlike oxygen isotope ratios here, a new method termed "clumped isotope thermometry" is not dependent on knowing or assuming the oxygen isotope composition of the water at the time a mineral or biomineral grew.²⁰ Validation of the angle-spread proxy in ancient fossil nacre, therefore, should be done with clumped isotope thermometry and angle spread measurements

on the same sample. If the results are found to be in agreement, nacre-paleothermometry will be established.

4 Experimental

4.1 Samples

The *Nautilus pompilius* shell (*Np*, 183 mm maximum length) originated off the coast of Siquijor Island, Philippines, and was purchased from Conchology Inc., Philippines. The *Np* sample was collected from the outer wall of the largest chamber, not from a septum. *Haliotis iris* (*Hi*, 107 mm maximum length), the paua shell, or blackfoot abalone from New Zealand, was purchased from Australian Seashells PTY Ltd.

The *Pinctada margaritifera* shell (*Pm*, 90 mm maximum length) was purchased at the Gauguin Pearl Farm, Rangiroa, French Polynesia.

All three shells in Fig. 1 were cut with hammer and chisel, to a final size of approximately 1 cm. One side of each square sample was coarsely polished with sandpaper, and then adhered to double-stick tape for accurate vertical mounting of the cross-sections. The samples were then embedded in epoxy (EpoThin, Buehler, IL) and polished with decreasing size alumina grit down to 50 nm (MasterPrep, Buehler, IL). Sample surfaces were coated using a sputter coater (208HR, Cressington, UK) with 40 nm of platinum while the region to be analyzed by PEEM was masked off, and a final coating of 1 nm platinum was applied to the entire surface to prevent charging.²⁷

The *Pm* shell sample analyzed with SIMS and PEEM was extracted with hammer and chisel and one side was coarsely polished with sandpaper for accurate vertical mounting of the cross-section. The sample was then baked for 1 h at 310 °C to remove the organic material. The baked shell sample was embedded in epoxy (EpoxyCure, Buehler, IL), with grains of UWC-3 calcite standard⁸ cast in the center of the sample mount, and the sample was polished with sandpaper and alumina grit. Care was taken to reduce surface topography and polishing relief, including applying a thin layer of epoxy to the partially polished surface to fill cracks and bubbles.

4.2 XANES-PEEM analysis

X-Ray photoelectron emission spectromicroscopy was performed using the PEEM-3 microscope, on the 11.0.1 beamline at the Advanced Light Source in Berkeley, CA. The elliptically polarizing undulator (EPU) at this beamline was calibrated to provide precise linear X-ray polarization and reproducible intensities at polarization angles between 0–90° with a 5° step size.

4.3 PIC-maps

The methods for PIC-mapping are described in detail in ref. 2*f* and 5. Briefly, we define the *c'*-axis as the projection of the CaCO₃ *c*-axis onto the EPU polarization plane. Separate PEEM images were acquired at each EPU polarization angle from 0–90° by 5° steps, a total of 19 images for each nacre region. For all the images the sample voltage was –15 kV and the photon energy was kept constant at 290.3 eV, the carbon K-edge π^* peak,²⁸ which is the peak most sensitive to the linear polarization angle.⁵ All images were 20 $\mu\text{m} \times 20 \mu\text{m}$ in size, with 20-nm pixels. For each pixel, if the intensities in each of these 19 images are plotted against the corresponding EPU polarization angle, the resulting curve follows a cosine-squared function where the position of the curve maximum indicates the angle at which the *c'*-axis is aligned parallel to the EPU polarization angle.⁵ Fitting these data to the curve $y = A + B \cos^2(EPU^\circ + \theta)$, with the Levenberg–Marquardt least-squares analysis method, yields accurate identification of the position of the curve maximum and thereby determination of *c'*-axis orientation. Performing this fit for every 20-nm

pixel in the stack of 1030×1054 -pixel images obtained from PEEM-3, and composing the results into a single gray scale image yields a PIC-map, in which the c' -axis orientation angle is quantitatively represented by a gray level between 0–255. These gray levels correspond to the possible 180° -range of orientations between -90° and $+90^\circ$, with 0° corresponding to a vertical c' -axis. Note that all c' -axes point around the normal, thus only the $\pm 45^\circ$ range is shown in Fig. 1 and 2.

The procedures used to obtain the PIC-maps were developed by one of us (I.C.O.) in WaveMetrics Igor Pro 6.2[®], and are available to any interested users free of charge on our web site (see “GG Macros”).²⁹

4.4 Angle spread

The physical quantity we measure in PIC-maps is the projection (termed c' -axis) of the c -axis onto the EPU polarization plane.^{2,5} If the c -axes of two nacre tablets are perfectly co-oriented, their c' -axes will also be co-oriented. If the c -axes of two nacre tablets are differently oriented, then their c' -axes are almost always differently oriented. The only ambiguous case is the following: if the c -axes of two tablets point in different directions in three-dimensional space, and these directions are in a plane perpendicular to the plane in which the X-ray polarization rotates, then their c' -axes will appear the same in PIC-maps, whereas the c -axes are in reality distinct. This is the only ambiguous case because nacre tablets have their axes preferentially oriented perpendicular to the nacre planes, and depart from that direction by a maximum angle of $\pm 50.5^\circ$ (the maximum spread measured never exceeded 101° ²⁹). If these angles were as large as $\pm 90^\circ$, then two c -axes nearly perpendicular to the EPU plane could yield very large spreads in θ' angles, even though they are nearly co-oriented in three-dimensional space. Since this is never the case for a nacre cross-section sample, and the samples are always mounted with the nacre lines horizontal, the aforementioned is the only ambiguous case.

All data were collected in nacre regions far from the nacre-prismatic boundary in order to avoid the greater angle spreads that near-boundary regions would exhibit, resulting from the gradual ordering mechanism found in *Haliotis rufescens* nacre.³⁰ We note that the angle spread is a *maximum* spread between c' -axes orientations, and therefore any angles between the minimum and the maximum θ' angle (see histograms of Fig. 1) are included and consistently found in the data.

Measuring the “footprint” of the distribution of θ' angles in a PIC-map as shown in Fig. 1 is effective for representing the total spread of aragonite c' -axis angles across nacre tablets within a region. Footprint measurements were done from histograms in Igor Pro[®], displayed as “levels” for PIC-map images.²⁹ To increase the number of points in which the angle spread is measured, we sliced each $20 \mu\text{m} \times 20 \mu\text{m}$ region into five $4 \mu\text{m} \times 20 \mu\text{m}$ regions, as shown in Fig. 2. These were 68 $20\text{-}\mu\text{m}$ maps, which then became 340 PIC-maps. In retrospect, this was not a good choice, as the data turned out to be under-sampling the angle spreads, because there are too few tablets in a $4 \mu\text{m} \times 20 \mu\text{m}$ region to give stable and meaningful values of angle spreads. In other words, the histograms of smaller regions are not as symmetric and statistically representative as those shown in Fig. 1. Evidence of appropriate sampling for angle spread will manifest itself as single-peaked, symmetric histograms, approaching a Gaussian line shape much more than those obtained from the $20\text{-}\mu\text{m}$ fields of view in Fig. 1. This is why we wrote above that $80 \mu\text{m} \times 40 \mu\text{m}$ fields of view are required.

4.5 Oxygen isotope measurements by secondary ion mass spectrometry (SIMS)

Oxygen isotope measurements were performed by SIMS on the WiscSIMS CA-MECA ims-1280 high-resolution, multi-collector ion microprobe, at the University of Wisconsin-Madison^{2,7,4,31} using a $^{133}\text{Cs}^+$ beam with an intensity of 1.3 nA, focused to approximately $10 \mu\text{m}$ beam spot-size. Charging of the sample surface was

compensated by Au coating, and by using an electron flood gun. The general conditions were similar to those reported in ref. 7e. The secondary $^{16}\text{O}^-$ and $^{18}\text{O}^-$ ions were collected simultaneously by Faraday cup detectors with typical $^{16}\text{O}^-$ ion intensity of 2.3×10^9 cps. The total analytical time per spot was about 4 min, including pre-sputtering (10 s), automatic centering of the secondary ion image in the field aperture (*ca.* 1.5 min) and analysis (*ca.* 2 min).

Grains of UWC-3 calcite standard ($\delta^{18}\text{O} = 12.49\text{‰}$ [VSMOW])⁸ were measured in at least four spots before and after every 8–18 sample analyses, and the resulting average value of bracketing the samples was used for bias correction. The average precision (reproducibility) for a set of bracketing standards is $\pm 0.28\text{‰}$ (2 SD, spot-to-spot).

Oxygen isotope ratios of marine carbonates are traditionally expressed relative to PDB. Therefore, final data were converted from $\delta^{18}\text{O}$ on the VSMOW to the PDB scale by the equation of Coplen *et al.*:^{7b}

$$\delta^{18}\text{O}\text{‰ PDB} = 0.97002 \times \delta^{18}\text{O}\text{‰ VSMOW} - 29.98.$$

Acknowledgements

We thank beamline scientists Andreas Scholl, Anthony Young and Andrew Doran for their expert technical support during the PEEM-3 experiments. We thank Reinhard Kozdon and John W. Valley for their collaboration on the SIMS experiments and for reading this manuscript. We also thanks Brian Hess and John Fournelle for SIMS sample preparations and imaging. This work was supported by NSF awards CHE-0613972 and DMR-1105167, DOE Award DE-FG02-07ER15899, and UW-Hamel Award to PUPAG. The PEEM experiments were performed at the Berkeley Advanced Light Source, supported by DOE under contract DE-AC02-05CH11231. WiseSIMS is partially supported by NSF-EAR awards 0319230, 0744079, 1053466.

5 References

- (a) H. A. Lowenstam, *Science*, 1981, **211**, 1126–1131; (b) H. A. Lowenstam and S. Weiner, *On Biomineralization*, Oxford University Press, New York, 1989, p; (c) S. Mann, *Biomineralization: Principles and Concepts in Bioinorganic Materials Chemistry*, Oxford University Press, New York, 2001, p.
- (a) R. A. Metzler, M. Abrecht, R. M. Olabisi, D. Ariosa, C. J. Johnson, B. H. Frazer, S. N. Coppersmith and P. U. P. A. Gilbert, *Phys. Rev. Lett.*, 2007, **98**, 268102; (b) P. U. P. A. Gilbert, R. A. Metzler, D. Zhou, A. Scholl, A. Doran, A. Young, M. Kunz, N. Tamura and S. N. Coppersmith, *J. Am. Chem. Soc.*, 2008, **130**, 17519–17527; (c) R. A. Metzler, D. Zhou, M. Abrecht, J.-W. Chiou, J. Guo, D. Ariosa, S. N. Coppersmith and P. U. P. A. Gilbert, *Phys. Rev. B: Condens. Matter Mater. Phys.*, 2008, **77**, 064110–064111/064119; (d) D. Zhou, R. A. Metzler, T. Tyliczszak, J. Guo, M. Abrecht, S. N. Coppersmith and P. U. P. A. Gilbert, *J. Phys. Chem. B*, 2008, **112**, 13128–13135; (e) R. A. Metzler, J. S. Evans, C. E. Killian, D. Zhou, T. H. Churchill, N. P. Appathurai, S. N. Coppersmith and P. U. P. A. Gilbert, *J. Am. Chem. Soc.*, 2010, **132**, 6329–6334; (f) I. C. Olson, R. Kozdon, J. W. Valley and P. U. P. A. Gilbert, *J. Am. Chem. Soc.*, 2012, **134**, 7351–7358.
- (a) E. DiMasi and M. Sarikaya, *J. Mater. Res.*, 2004, **19**, 1471–1476; (b) K. Gries, R. Kröger, C. Kübel, M. Schowalter, M. Fritz and A. Rosenauer, *Ultramicroscopy*, 2009, **109**, 230–236; (c) A. G. Checa, J. H. E. Cartwright and M. G. Willinger, *J. Struct. Biol.*, 2011, **176**, 330–339.
- (a) Y. R. Ma, B. Aichmayer, O. Paris, P. Fratzl, A. Meibom, R. A. Metzler, Y. Politi, L. Addadi, P. U. P. A. Gilbert and S. Weiner, *Proc. Natl. Acad. Sci. U. S. A.*, 2009, **106**, 6048–6053; (b) C. E. Killian, R. A. Metzler, Y. T. Gong, I. C. Olson, J. Aizenberg, Y. Politi, L. Addadi, S. Weiner, F. H. Wilt, A. Scholl, A. Young, S. N. Coppersmith and P. U. P. A. Gilbert, *J. Am. Chem. Soc.*, 2009, **131**, 18404–18409.
- P. U. P. A. Gilbert, A. Young and S. N. Coppersmith, *Proc. Natl. Acad. Sci. U. S. A.*, 2011, **108**, 11350–11355.

-
- 6 NOAA in *Pacific Marine Environmental Laboratory Tropical Atmosphere Ocean Project. Data buoy at 155W 8S*, Vol. 2011.
- 7 (a) H. C. Urey, *J. Chem. Soc.*, 1947, **1**, 562–581; (b) T. B. Coplen, C. Kendall and J. Hopple, *Nature*, 1983, **302**, 236–238; (c) E. L. Grossman and T.-L. Ku, *Chem. Geol.: Isot. Geosci. Sect.*, 1986, **59**, 59–74; (d) N. T. Kita, T. Ushikubo, B. Fu and J. W. Valley, *Chem. Geol.*, 2009, **264**, 43–57; (e) R. Kozdon, D. C. Kelly, N. T. Kita, J. H. Fournelle and J. W. Valley, *Paleoceanography*, 2011, **26**, PA3206.
- 8 R. Kozdon, T. Ushikubo, N. T. Kita, M. Spicuzza and J. W. Valley, *Chem. Geol.*, 2009, **258**, 327–337.
- 9 S.-T. Kim and J. R. O’Neil, *Geochim. Cosmochim. Acta*, 1997, **61**, 3461–3475.
- 10 (a) J. W. Morse, J. J. Zullig, L. D. Bernstein, F. J. Millero, P. Milne, A. Mucci and G. R. Choppin, *Am. J. Sci.*, 1985, **285**, 147–185; (b) P. Zuddas and A. Mucci, *Geochim. Cosmochim. Acta*, 1994, **58**, 4353–4362; (c) P. Zuddas and A. Mucci, *Geochim. Cosmochim. Acta*, 1998, **62**, 757–766.
- 11 L. Addadi and S. Weiner, *Proc. Natl. Acad. Sci. U. S. A.*, 1985, **82**, 4110–4114.
- 12 (a) D. Chateigner, C. Hedegaard and H. R. Wenk, *J. Struct. Geol.*, 2000, **22**, 1723–1735; (b) J. H. E. Cartwright and A. G. Checa, *J. R. Soc. Interface*, 2007, **4**, 491–504; (c) D. Chateigner, S. Ouhenia, C. Krauss, C. Hedegaard, O. Gil, M. Morales, L. Lutterotti, M. Rousseau and E. Lopez, *Mater. Sci. Eng., A*, 2010, **528**, 37–51.
- 13 (a) C. M. Zarella, A. M. Belcher, M. Fritz, Y. L. Li, S. Mann, P. K. Hansma, D. E. Morse, J. S. Speck and G. D. Stucky, *Chem. Mater.*, 1996, **8**, 679–690; (b) A. G. Checa and A. B. Rodríguez-Navarro, *Biomaterials*, 2005, **26**, 1071–1079.
- 14 E. Zolotoyabko, *J. Appl. Crystallogr.*, 2009, **42**, 513–518.
- 15 A. Pérez-Huerta, Y. Dauphin, J. P. Cuif and M. Cusack, *Micron*, 2011, **42**, 246–251.
- 16 H. Mutvei, *Biomíneralisation*, 1972, **4**, 81–86.
- 17 (a) H. A. Lowenstam, *J. Geol.*, 1954, **62**, 284–322; (b) H. A. Lowenstam, *Proc. Natl. Acad. Sci. U. S. A.*, 1954, **40**, 39–48.
- 18 (a) Y. Rosenthal and G. P. Lohmann, *Paleoceanography*, 2002, **17**; (b) H. Elderfield, J. Yu, P. Anand, T. Kiefer and B. Nyland, *Earth Planet. Sci. Lett.*, 2006, **250**, 633–649.
- 19 (a) P. L. Koch, *Annu. Rev. Earth Planet. Sci.*, 1998, **26**, 573–613; (b) S. Schouten, E. C. Hopmans, A. Forster, Y. van Breugel, M. M. M. Kuypers and J. S. S. Damste, *Geology*, 2003, **31**, 1069–1072.
- 20 R. A. Eagle, T. Tutken, T. S. Martin, A. K. Tripathi, H. C. Fricke, M. Connely, R. L. Cifelli and J. M. Eiler, *Science*, 2011, **333**, 443–445.
- 21 (a) A. W. H. Be, *Science*, 1968, **161**, 881–884; (b) W. E. Frerichs, M. E. Heiman, L. E. Borgman and A. W. H. Be, *J. Foraminiferal Res.*, 1972, **2**, 6–13.
- 22 Y. Dauphin, *Curr. Opin. Colloid Interface Sci.*, 2002, **7**, 133–138.
- 23 (a) H. Mutvei, *N. Jb. Geol. Paläont. Abh.*, 1967, **129**, 157–166; (b) C. A. McRoberts and J. G. Carter, *Journal of Paleontology*, 1994, **68**, 1405–1408.
- 24 (a) B. Runnegar, *Alcheringa: An Australasian Journal of Palaeontology*, 1985, **9**, 245–257; (b) C. M. Zarella, D. E. Morse, S. Mann, P. K. Hansma and G. D. Stucky, *Chem. Mater.*, 1998, **10**, 3813–3824.
- 25 S. M. Antao, *RSC Adv.*, 2012, **2**, 526–530.
- 26 (a) H. Mutvei, *Lethaia*, 1983, **16**, 233–240; (b) H. Mutvei and E. Dunca, *Paläontologische Zeitschrift*, 2010, **84**, 457–465; (c) M. J. Vendrasco, A. G. Checa and A. V. Kouchinsky, *Palaeontology*, 2011, **54**, 825–850.
- 27 (a) B. Gilbert, R. Andres, P. Perfetti, G. Margaritondo, G. Rempfer and G. De Stasio, *Ultramicroscopy*, 2000, **83**, 129–139; (b) B. H. Frazer, B. Gilbert, B. R. Sonderegger and G. De Stasio, *Surf. Sci.*, 2003, **537**, 161–167; (c) G. De Stasio, B. H. Frazer, B. Gilbert, K. L. Richter and J. W. Valley, *Ultramicroscopy*, 2003, **98**, 57–62; (d) P. U. P. A. Gilbert, B. H. Frazer and M. Abrecht in *The organic-mineral interface in biominerals*, Vol. 59 ed.: J. F. Banfield, K. H. Nealson and J. Cervini-Silva, Mineralogical Society of America, Washington DC, 2005, p. 1570185.
- 28 R. A. Metzler, M. Abrecht, R. M. Olabisi, D. Ariosa, C. J. Johnson, B. H. Frazer, S. N. Coppersmith and P. Gilbert, *Phys. Rev. Lett.*, 2007, **98**, 268102.
- 29 GG-Macros, <http://home.physics.wisc.edu/gilbert/> 2011.
- 30 P. U. P. A. Gilbert, R. Metzler, D. Zhou, A. Scholl, A. Doran, A. Young, M. Kunz, N. Tamura and S. Coppersmith, *J. Am. Chem. Soc.*, 2008, **130**, 17519–17527.
- 31 J. W. Valley and N. T. Kita in *In situ oxygen isotope geochemistry by ion microprobe*, Vol. 41, ed. M. Fayek, 2009, pp. 16–63.
-